JES Focus Issue Honoring Allen J. Bard

Film Permeation by Rotating Disk Voltammetry at Electrodes Modified with Electrochemically Inert Layers and Heterogeneous Composites

Krysti L. Knoche,* Chaminda Hettige,* Lois Anne Zook-Gerdau, and Johna Leddy,z**

Department of Chemistry, University of Iowa, Iowa City, Iowa 52242, USA

Steady state rotating disk voltammetry provides excellent measurement of permeability for films and layers on electrodes because the hydrodynamic control of rotating disks establishes well defined boundary layers normal to the electrode. For a redox probe present in solution and pre-equilibrated in the layer, voltammetry measures electrolysis current for the probe as the probe transports from solution, through the film, and to the electrode where the probe is electrolyzed. Diagnostic equations relate the steady state, mass transport limited current i_{ss} to the rotation rate ω. The incompressible layer is electroinactive about the probe formal potential. Diagnostics are available for a single layer, uniform film (Gough and Leypoldt). Uniform films are homogeneous with no structural features. Here diagnostics are provided for bilayer and multilayer uniform films, where multilayers include discretely and continuously graded films. Consideration of serial mass transport resistances normal to the electrode allows diagnostics for uniform films. Heterogeneous, micro- and nano-structured layers are structured in the plane of the electrode. Consideration of parallel mass transport resistances as part of the layer mass transport resistance yields diagnostics for heterogeneous films. Diagnostics are vetted with literature data. Theoretical and practical advantages and limitations are noted.

Manuscript submitted November 23, 2015; revised manuscript received February 12, 2016. Published February 24, 2016. *This paper is part of the JES Focus Issue Honoring Allen J. Bard.*

Rotating disk voltammetry is often used to evaluate electrodes modified with incompressible films of various materials.[1–10] In steady state rotating disk measurements, redox probe present in solution is transported from solution through the inert film to the electrode where the probe is electrolyzed. Because probe interactions with the film limit flux through the film, flux maps film structure and properties; steady state currents measure flux. An inert film is electroinactive in the voltage range where the redox probe is electrolyzed. Inert films include electrochemically silent layers and ion exchange polymers. Redox and electron conducting polymers are inert outside potential ranges where the polymer itself is electrolyzed. Some micro- and nano-structured, heterogeneous films are inert. Porous, electrochemically silent layers include supports for heterogeneous catalysts and electrodes as well as particles such as zeolites formed into a coherent layer. In pharmaceutical and biomembrane studies, radiotracer measurements are commonly employed, but rotating disk allows better measures of permeability because the refined hydrodynamic control establishes well defined steady state boundary layers.

Rotating disk voltammetry establishes excellent hydrodynamic control of flux normal to the electrode.[11] Control of flux is exploited to determine film permeability. Voltammetric diagnostics of steady state flux through a single, electroinactive, uniform layer are reported.[12–15] The single layer and solution each establish a mass transport resistance for the probe that limits flux and measured current. Comparison of flux (current) at modified and unmodified electrodes measures film mass transport resistance and permeability.

Here, equations are presented for steady state permeation of redox probes through inert films that are composed of more than a single layer. Bilayers may be formed by successive coatings or as a natural consequence of a crust forming at the film solution interface. Multilayers, which may also be formed by successive coatings, serve as models for both discretely layered and continuously graded films. Equations are derived for uniform films from linearized concentration profiles and from serial mass transport resistances normal to the electrode surface. Rotating disk voltammetry alone yields only the effective permeability of the layers. Additional information is needed to further deconvolve the thicknesses, diffusion coefficients, and partition parameters that characterize permeability. Without additional information, an effective permeability for the entire layer is found for single, bi- and multi-layers. Additional characterization includes independent film evaluations (e.g., microscopy, ellipsometry,[16] and electrochemical quartz crystal microbalance[17,18]); voltammetric protocols that vary experimental parameters (e.g., layer thicknesses); and coupling steady state voltammetry with transient methods (e.g., chronoamperometry and cyclic voltammetry[19]).

Uniform films are homogeneous. Only flux normal to the electrode and serial resistances are needed to model uniform layers. Microstructured, heterogeneous and porous films have structures that vary in the plane of the electrode, which disrupt transport normal to the electrode. Here, equations for permeability of microstructured and porous layers are developed on inclusion of parallel transport paths (parallel mass transport resistances) within the layer. Limitations of rotating disk measurements, such as statistical constraints, times to establish steady state, and failure of the methodology are discussed. Literature data are used to illustrate the various methodologies outlined for steady state rotating disk voltammetry at electrodes modified with electrochemically inert layers, both uniform and heterogeneous.

Rotating Disk Experiments

Macroscopically, when a flat, unmodified electrode is rotated, fluid flows from the bulk toward and normal to the electrode surface.[11,20] Immediately at the electrode surface, solvent and electrolyte species are carried with the rotating electrode. The surface layer drags the adjacent fluid layer and so with subsequent layers for a substantial distance such that a stagnant layer is established at the electrode surface. To a reasonable approximation, transport in the stagnant layer occurs only by diffusion. Outside of this layer, solution is moved by convection. For convection-diffusion in an isotropic, incompressible fluid under laminar (non-turbulent) flow, the thickness of the stagnant or boundary layer, δ_0 (cm), is well approximated as

$$\delta_0 = 1.61\nu^{1/6}D_s^{1/3}\omega^{-1/2} \quad [1]$$

*Electrochemical Society Student Member.
**Electrochemical Society Fellow.
zE-mail: johna-leddy@uiowa.edu

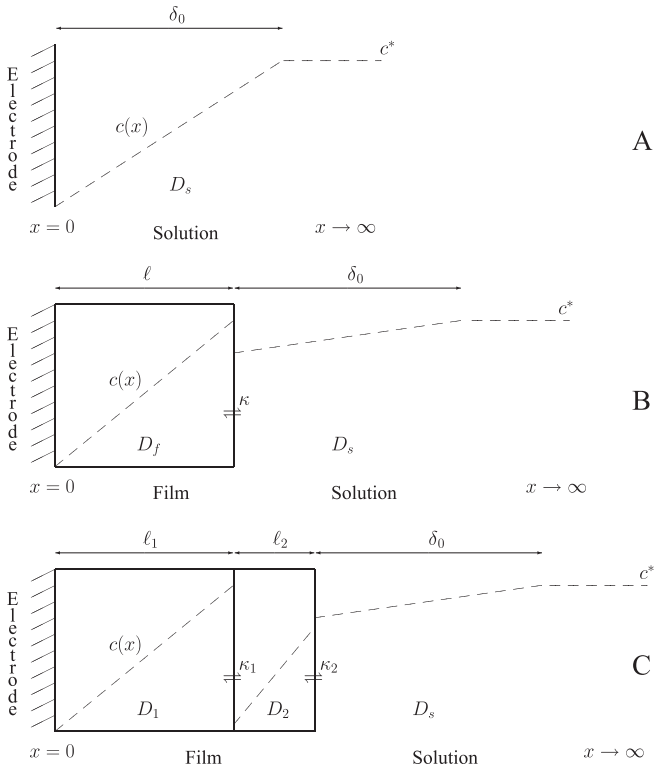

Figure 1. Linearized concentration profiles, $c\,(x)$, for three steady state cases. For serial mass transport resistances, steady state is achieved when the concentration profiles, shown as dashed lines, are linear. (A) For an unmodified electrode; (B) for an electrode modified with a single layer, uniform film, shown for $\kappa > 1$ and $D_f < D_s$; and (C) for an electrode modified with a bilayer, shown for the outer layer as a crust, where $\kappa_1 \gg 1$, $\kappa < 1$, and $D_s > D_1 > D_2$.

Rotation rate, ω, is expressed in radians per second. For a rotational frequency, f, in rotations per minute, $\omega = 2\pi f/60$. Probe diffusion coefficient in solution is D_s (cm^2/s). Kinematic viscosity, ν is the ratio of the solution viscosity to solution density, (cm^2/s). Boundary layer thickness decreases with ω. For water at 25°C, $\nu = 0.00893$ cm^2/s; for typical D_s of 8×10^{-6} cm^2/s and $f = 1000$ rpm ($\omega = 105$ s^{-1}), δ_0 is 15 μm; for $f = 100$ rpm, δ_0 is 46 μm.

Levich developed the current expression for steady state, mass transport limited electrolysis at a rotating disk. The Levich equation derives from a linearized approximation of diffusion through the stagnant layer. Let the coordinate normal to the electrode surface be x. For a redox probe in solution at bulk concentration c^* (mol/cm^3) and electrolyzed at the electrode surface ($x = 0$) at the mass transport limited rate ($c\,(x = 0) = 0$), a steady state concentration profile $c\,(x)$ is well-approximated linearly as shown in Figure 1A. Steady state flux in solution, J_{soln}, at $x = 0$ sets steady state current in solution, i_{soln}. In Equation 2, the discretized approximation to $dc(x)/dx$ is shown. For electrolysis at the mass transport limit, $c(0) = 0$, the Levich equation is shown in Equation 3.

$$\frac{i_{\text{soln}}}{nFA} = -J_{\text{soln}}\,(x = 0) = D_s \left.\frac{dc\,(x)}{dx}\right|_{x=0} = D_s \frac{c^* - c(0)}{\delta_0} \qquad [2]$$

$$\left.\frac{i_{\text{soln}}}{nFA}\right|_{Levich} = D_s \frac{c^*}{\delta_0} = 0.62 c^* D_s^{2/3} \nu^{-1/6} \omega^{1/2} \qquad [3]$$

n, F, and A are the number of electrons transferred ($O + ne \rightleftharpoons R$), Faraday constant, and the geometric area of the electrode. For an unmodified electrode, the experimental, steady state current i_{ss} measures only flux in solution (i_{soln}). A Levich plot of i_{ss} versus $\omega^{1/2}$ will be linear. A double reciprocal plot, a Koutecky Levich plot, of i_{ss}^{-1} versus $\omega^{-1/2}$ is common and will yield a slope characteristic of transport in solution and, independent of any other limits on the current, an intercept of zero. For an unmodified electrode, a Levich plot that flattens at higher ω indicates current limited by effects other than mass transport in solution. A linear Koutecky Levich plot embeds this limiting, ω-independent information in the intercept. Embedding of ω-independent data in the intercept of the Koutecky Levich plot forms the basis for characterization of films on electrodes.

There are several practical considerations to good rotating disk measurements at unmodified electrodes. (i) To maintain laminar flow in a simple electrochemical cell, f is typically limited to less than a few thousand rotations per minute. (ii) For unmodified electrodes, $f > 50$ to 100 rpm establish boundary layers sufficient to avoid disruption by density and thermal gradients. (iii) Electrodes are best centered in a straight shaft. (iv) For a disk of radius r, an insulating shroud around the disk should be at least r thick to minimize radial diffusion not considered in the Levich equation derivation. (v) Disk radius r at least several fold larger than δ_0 further establishes linear diffusion as the only significant transport process. (vi) A well executed rotating disk experiment typically allows three significant figures in the current. (vii) At an unmodified electrode, it is common to sweep potential slowly ($\lesssim$ 10 mV/s) to map current from zero to the mass transport limited rate. A potential sweep for each ω is practical because steady state is rapidly established at unmodified electrodes.

General notes about rotating disk at modified electrodes.—When rotating disk experiments are performed at an electrode modified with a layer of thickness ℓ, the stagnant layer forms in solution just as at an unmodified electrode. The stagnant layer is still of thickness δ_0, but instead of being formed between $x = 0$ and $x = \delta_0$, δ_0 is formed between $x = \ell$ and $x = \ell + \delta_0$. Transport in the stagnant layer and the modifying layer is by diffusion. At steady state, flux in the film and flux in the solution must be equal.

Practical consideration for modified electrodes include those for unmodified electrodes and several specific to films. (i) Modifying layers must be incompressible. (ii) Thickness ℓ does not affect measurement quality provided the uniform layer is isotropic and time to steady state is not prohibitive. (iii) Time to steady state for a uniform film scales as $t_{ss} \propto \ell^2/D_f$ where D_f is the diffusion coefficient in the layer; typically, steady state is achieved when $t_{ss} \gtrsim 5\ell^2/D_f$, where t_{ss} can be long because $D_f < D_s$. (iv) Because t_{ss} can be much longer for a modified electrode, rotating disk measurements are often made by holding the potential at the mass transport limit ($c(0) = 0$) and waiting for steady state at some ω. Once i_{ss} is established constant, ω can be changed without changing the potential. Again, steady state must be established, but the time required is less than under potential sweep. (v) Data recorded in random ω order tends to prevent incorporation of film degradation as a systematic error. (vi) As for unmodified electrodes, cavitation sets the upper limit on ω. From practical experience, however, f as low as a few rpm can be used at modified electrodes, especially when flux in the film sets i_{ss}. (vii) To avoid radial diffusion in the film, the layer should completely cover but not extend beyond the electrode area. This is typically not difficult for hydrophobic electrodes shrouds (e.g., polytetrafluoroethylene (PTFE)) and films that allow probe diffusion from a higher dielectric constant electrolyte. Films may swell in the electrolyte, but cannot dissolve or detach from the electrode. Because electrochemical solvents cover a range of dielectric constants (e.g., 78 for water, 37 for acetonitrile, and 9 for dichloromethane), a solvent can usually be found. Some films, especially polymers, swell to different extents in different solvents.

Because of well controlled transport (δ_0), rotating disk methods characterize films with greater precision than concentration cells used in permeation studies. Steady state voltammetry is an attractive and more accurate alternative to radiotracer studies of films and coatings used, for example, in pharmaceutical and coating studies.

Models for Uniform Films

For modified electrodes, the steady state, linear approximation to the boundary layer thickness in solution, δ_0, remains. At steady

state, Fick's second law $(\partial c(x,t)/\partial t = 0 = D\partial^2 c(x,t)/\partial x^2 = -\partial J(x,t)/\partial x)$ dictates flux in solution and flux through each layer of the film must be equal.

For uniform films, each layer is homogeneous, isotropic, and incompressible. Uniform layers are without structure in the plane parallel to the electrode. Films may be composed of one (single layer), two (bilayer), or more (multilayer) layers. Multilayers can be discrete or continuous. Each uniform layer is characterized by thickness, transport, and concentration. Generally, the film is confined to the area A of the electrode to eliminate steady state radial flux in the film and the cross sectional area of the film (A) is large compared to the film thickness ℓ. For uniform films, rotating disk measurements yield at least an effective permeability or viscosity.

Uniform films are defined as electrochemically inert layers. The film itself is either electroinactive or probe electrolysis is undertaken at a potential range where the film is not electrolyzed. For example, Nafion is not electroactive but the probes that diffuse through Nafion can be electrolyzed. Redox polymers can be studied in potential ranges where the monomer units are not themselves electroactive but a redox probe is.

Single layer, uniform films.—Gough and Leypoldt[12–15] first derived the steady current measured for the electrolysis of a redox probe transported from solution through an electroinactive, uniform, single layer film to the electrode surface. Film is characterized by thickness ℓ and probe diffusion coefficient D_f. The probe present in solution at concentration c^* is equilibrated in the film prior to measurement. Film concentration is reported as the equilibrium ratio of the probe between the solution and film, characterized as

$$\kappa = \frac{c(\ell^-)}{c(\ell^+)} \qquad [4]$$

$c(\ell^-)$ and $c(\ell^+)$ are probe concentrations just inside and outside the film solution interface located at $x = \ell$. Note, κ also parameterizes the probe concentration in the film relative to the solution prior to electrolysis. κ is not a true equilibrium constant. If the concentration in the film is fixed independent of c^*, as it may be for an ion exchange polymer, then the parameter κ will vary with c^*. Steady state concentration profiles for single layer, uniform films are illustrated in Figure 1B, where as drawn, $\kappa > 1$ and diffusion coefficient in the solution is higher than in the film.

Specification by flux balance.—At steady state in a uniform film, flux through every plane parallel to the electrode surface is equal. By Fick's second law in one dimension, if the fluxes are not equal, spatial variation in flux will lead to a time dependent variation in concentration inconsistent with steady state. Flux in the film and solution are equal. Consider interfaces where flux is well specified: the electrode surface and the film solution interface.

$$\frac{i_{ss}}{nFA} = D_f \frac{dc(x)}{dx}\bigg|_{x=0} = D_s \frac{dc(x)}{dx}\bigg|_{x=\ell^+} \qquad [5]$$

Discretized, linear approximation of the gradients and incorporation of Equation 4 yields

$$\frac{i_{ss}}{nFA} = D_f \frac{c(\ell^-) - c(0)}{\ell} = D_s \frac{c(\ell + \delta_0) - c(\ell^+)}{\delta_0}$$
$$= D_s \frac{c(\ell + \delta_0) - c(\ell^-)/\kappa}{\delta_0} \qquad [6]$$

The concentration at $\ell + \delta_0$ is c^*. For electrolysis at the mass transport limited rate, $c(0) = 0$. Equation 6 is solved to find $c(\ell^-) = \frac{D_s c^*}{\delta_0}\left[\frac{D_f}{\ell} + \frac{D_s}{\kappa\delta_0}\right]^{-1}$. (For potential controlled, steady state electrolysis where $c(0) \geq 0$, see Reference 21 for both simple permeation and various kinetic mechanisms.) Substitution of $c(\ell^-)$ yields

$$\frac{i_{ss}}{nFA} = \frac{D_f}{\ell}\left[\frac{\frac{D_s c^*}{\delta_0}}{\frac{D_f}{\ell} + \frac{D_s}{\kappa\delta_0}}\right] = \frac{D_s c^*}{\delta_0}\left[\frac{\frac{\kappa D_f}{\ell}}{\frac{\kappa D_f}{\ell} + \frac{D_s}{\delta_0}}\right] \qquad [7]$$

This yields a Levich plot (i_{ss} vs $\omega^{1/2}$) that approaches ω-independence at high ω. Data analysis is simplified by a Koutecky Levich plot, the reciprocal of Equation 7.

$$\frac{nFAc^*}{i_{ss}} = \frac{\delta_0}{D_s} + \frac{\ell}{\kappa D_f} \qquad [8]$$

The plot $nFAc^* i_{ss}^{-1}$ vs $\omega^{-1/2}$ yields a slope characteristic of transport in solution and an ω-independent intercept characteristic of transport in the film. The slope is $[0.62 D_s^{2/3} \nu^{-1/6}]^{-1}$ and the intercept is $\ell/\kappa D_f$. For the same A and c^*, the slopes of $nFAc^* i_{ss}^{-1}$ versus $\omega^{-1/2}$ should be the same for the unmodified and modified electrodes. Similar slopes serve as a check that the measurements are made in an appropriate manner and that i_{soln} is ω-dependent and i_{film} is ω-independent. Flux in the film J_{film} is represented as a current, $i_{film} = -nFAJ_{film}$. The permeability of the film, $P_{film} = \kappa D_f/\ell$, is found from the inverse intercept. If film and solution flux are expressed as the corresponding currents,

$$\frac{1}{i_{ss}} = \frac{1}{i_{\text{soln}}} + \frac{1}{i_{film}} \qquad [9]$$

A sufficiently small current, i_{soln} or i_{film} can dominate the measured i_{ss}.

Specification by resistance.—Equation 9 also derives from mass transport resistance. Redox probes move through solution to the film solution interface and through the film to the electrode surface, where probes undergo mass transport limited electrolysis. On motion through the film and the solution, the probe is subject to mass transport resistances R_{film} and R_{soln}. For transport across the film solution interface facile, the interface introduces no resistance. Transport is normal to the electrode and the resistances are in series for total resistance, $R_{Total} = R_{\text{soln}} + R_{film}$. As in Ohm's law, resistance and current are inversely related, so $i_{ss}^{-1} = i_{\text{soln}}^{-1} + i_{film}^{-1}$ (Equation 9). This requires that all currents flow through the same area (A) subject to the same driving force.

Data analysis.—The intercept of the Koutecky Levich plot yields permeability $P = \kappa D_f/\ell$. To separate parameters κ, D_f, and ℓ, additional information is needed. Transient voltammetry, such as chronoamperometry and cyclic voltammetry yield $\kappa\sqrt{D_f}$. If the transient experiment is executed for time sufficient that the diffusion length exceeds ℓ, ℓ^2/D_f is also found. The equation for the chronoamperometric response for permeation of a probe through an inert, single layer, uniform film is reported by Peerce and Bard.[22] A method to extract $\kappa\sqrt{D_f}$ and ℓ^2/D_f from cyclic voltammetry is reported by Knoche et al.[23] Given $P = \kappa D_f/\ell$, $\kappa\sqrt{D_f}$ and perhaps ℓ^2/D_f, the three parameters κ, D_f, and ℓ cannot be determined individually without additional information. Typically, this is ℓ.

Because films swell in solvents, the values of ℓ are frequently poorly determined. Often, the amount of material on the electrode is better specified in other ways. The mass of material on the electrode m (g) is determined either by the amount of material delivered to the electrode or by microbalance methods. Spectroscopy, coulometry, and titration yield probe surface coverage Γ (mol/cm^2). Neither m nor Γ suffice to separate the three parameters. However, if permeability $P = \kappa D_f/\ell$ is measured for several values of m or Γ, then other specification of transport through the film can be found. If Pm/A is invariant with m, then Pm/A has units of viscosity (g/cm s). Similarly, if $P\Gamma$ is invariant with Γ, then $P\Gamma$ has units mol/cm s.

Consider an interfacial resistance to transport at the film solution interface, $R_{\text{interface}}$, where $R_{\text{interface}}$ is independent of ℓ. Then, $R_{Total} = R_{\text{soln}} + R_{film}(\ell) + R_{\text{interface}}$ so that a Koutecky Levich plot of $i_{ss}^{-1} = i_{\text{soln}}^{-1} + i_{film}(\ell)^{-1} + i_{\text{interface}}^{-1}$ yields an intercept of

$i_{film}(\ell)^{-1} + i_{\text{interface}}^{-1}$ where $i_{film}(\ell)^{-1} \propto \ell$.[24] If ℓ is varied, then a plot of the measured $i_{film}(\ell)^{-1} + i_{\text{interface}}^{-1}$ versus ℓ will yield a slope proportional to κD_f and positive intercept proportional to $R_{\text{interface}}$. Here, $R_{\text{interface}}$ characterizes transport across the film solution interface, but the measurement yields any ℓ-independent resistance through any plane parallel to the electrode. The measurement does not distinguish interfacial charge transfer, resistance at $x = 0$ from interfacial mass transport resistance at $x = \ell$.

Examples.—Rotating disk voltammetry is commonly used to characterize single, electroinactive, uniform films on electrodes, as for examples, in studies from Allen J. Bard's labs.[19,24–32] Other literature reports for single, incompressible layers include clay and nanostructured clay composites, emulsion polymers and copolymers, latex, and redox polymers (where the redox potential of the probe is well separated from the electroactive monomer). Cases where $R_{\text{interface}} > 0$ are discussed below.

Example 1: Rotating disk voltammetry[33] of montmorillonite clay and clay + PVA (poly(vinyl alcohol)) composites 5:1 and 5:2 by weight on basal plane pyrolytic graphite were evaluated for probe of 1 mM $Mo(CN)_8^{4-}$ in 0.2 M sodium triflate. Film thickness ℓ was either calculated from known clay density or profilometry on wetted films. Levich plots approach a limiting current at higher ω. Koutecky Levich plots have the same slope as the unmodified electrode. Plots of $nFAc^*\kappa D_f/\ell$ vs ℓ^{-1} are linear with zero intercepts, consistent with $R_{\text{interface}} = 0$. Slopes yield κD_f that are reported to increase with PVA content as clay ($(1.1 \pm 0.2) \times 10^{-8}$ cm^2/s) < clay + PVA (5:1) ($(2.2 \pm 0.7) \times 10^{-8}$ cm^2/s) < clay + PVA (5:2) ($(25.6 \pm 3.0) \times 10^{-8}$ cm^2/s).

Example 2: Various acrylate emulsion polymers were evaluated for permeability and pinholes by Hall and coworkers by rotating disk voltammetry.[34] Emulsion polymers and copolymers were formed of methyl methacrylate (MMA), glycidyl methacrylate (GMA), and butyl acrylate (BA) with poly(vinyl alcohol) stabilizer. Four stable films of MMA:GMA:BA were formed in varying component ratios: Poly 12 (65:0:35), Poly 14 (35:0:65), Poly X1 (0:35:65), and Poly X6 (0:0:100). The redox probe was 1 mM tetramethyl-o-phenylenediamine (TMPD) in KCl, phosphate buffer at pH 7.0 and the electrode was 0.1141 cm^2 Pt. Permeability was reported as a function of mass of emulsion on the electrode as shown in Table I. Where pinholes were found according to the model of Landsberg and Thiele,[35] an x is shown in the Table. Added to the Table is $P(m/A)$ for each emulsion. The units of Pm/A are g/cm s, the units of viscosity, where 0.01 g/ cm s is 1 centipoise. Where P varies with m/A, Pm/A does not vary systematically with m/A so Pm/A provides an intensive metric to compare the polymers. Average values of Pm/A are shown with standard deviations. In all cases, median Pm/A is comparable to average Pm/A. The values of Pm/A are similar for all emulsions, averaging to 3×10^{-4} cp, which is well below the viscosity of water (1 cp). The intensive Pm/A is then a good figure of merit for these films but not a direct measure of the film viscosity.

Table I. Permeability (10^{-3} cm/s) of TMPD through Four Emulsions. P of TMPD is reported with mass of the emulsion per area m/A (mg/cm^2).[34]

	Mass/Area m/A emulsion (mg/cm^2)	Permeability P (10^{-3} cm/s)	Pm/A (10^{-6} g/cm s)	Pm/A (Average ± st dev) (10^{-6} g/cm s)
Poly 12	1.10	5.32	5.85	
(65:0:35)	2.19	1.32	2.96	(4 ± 2)
	3.33	x		
	4.39	x		
Poly 14	1.10	2.28	2.51	
(35:0:65)	2.19	1.07	2.34	
	4.39	0.703	3.09	(2.6 ± 0.4)
	8.78	x		
Poly X1	0.53	3.43	1.82	
(0:35:65)	1.10	2.21	2.43	
	2.19	1.51	3.31	
	3.33	0.95	3.16	
	4.39	0.89	3.91	(2.9 ± 0.8)
	6.58	x		
Poly X6	1.10	3.92	4.31	
(0:0:100)	2.19	1.30	2.85	
	4.39	0.833	3.66	
	6.58	0.547	3.60	(3.6 ± 0.6)

Example 3: Cosnier et al.,[36] measured permeabilities of $Fe(CN)_6^{4-}$ through layers of latex (5-hydroxymethyl-bicyclo[2.2.1]-hept-2-ene) where the latex layers are applied in volume increments that each add 0.250 mg of latex per 0.20 cm^2. Measured permeabilities P (10^{-4} cm/s) are reported as 16.2, 8.10, and 5.40 for 1, 2, and 3 layers. The product of measured P with the number of layers is fixed (1.62×10^{-3} cm/s), so that the latex is intensively parameterized with the invariant, effective viscosity (2.06 μg [cms]$^{-1}$), independent of the number of layers.

Example 4: Interfacial resistance was evaluated for several redox polymers by plotting measured P^{-1} versus ℓ, where a positive intercept characterizes $R_{\text{interface}}$.[24] Where Koutecky Levich slopes were the same as for the unmodified electrodes and positive intercepts were found from measured P^{-1} versus ℓ, interfacial rates were in the range of 0.01 to 0.1 cm/s. These data were for electroactive polymers such as poly[$(Ru(vbpy)_3]^{2+}$, poly[VDQ]$^{2+}$, poly[$Ru(bpy)_2$(p-cinn)$_2]^{2+}$,[37] and poly(vinyl ferrocene)[19] in acetonitrile with redox probes such as benzoquinone and ferrocene; VDQ is vinyl diquat, vbpy is a vinyl bipyridine, and p-cinn is N-(4-pyridine)cinnamamide. Yet slower rates of interfacial transport may be sufficient to alter the slope of the Koutecky Levich plots; see statistical limitations in the measurements in Statistical limitations section. Negative intercepts of measured P^{-1} versus ℓ do not correspond to any known models of transport (and coupled transport-kinetics) for incompressible films, but can reflect statistically insignificant intercepts and inconsistency in the measurements and analysis. When intercepts of P^{-1} versus ℓ are negative, interfacial mass transport resistance likely does not dominate limitation to the measured current.

Bilayers, two uniform layers.—Bilayers may be formed when two layers are sequentially applied to an electrode or when a film develops a crust, such as might be observed as latex paint dries. Steady state concentration profiles for a bilayer are shown in Figure 1C. The layer nearest the electrode is of thickness ℓ_1 and diffusion coefficient D_1. A ratio of concentration between the first and second layer characterized yields $\kappa_1 = c(\ell_1^-)/c(\ell_1^+)$. Similarly, for the outer layer, ℓ_2, D_2, and $\kappa_2 = c(\ell_1 + \ell_2^-)/c(\ell_1 + \ell_2^+)$ apply.

Specification by flux balance.—Equations for a bilayer develop analogously to a single layer. Equal flux through each plane parallel to the electrode is required. For three interfaces: at the electrode $x = 0$, between the first and second layer $x = \ell_1$ and between the outer layer and the solution $x = \ell_2$:

$$\frac{i_{ss}}{nFA} = D_1 \frac{dc(x)}{dx}\bigg|_{x=0} = D_2 \frac{dc(x)}{dx}\bigg|_{x=\ell_1^+} = D_s \frac{dc(x)}{dx}\bigg|_{x=\ell_1+\ell_2^+} \quad [10]$$

Discretized, linear approximations for the gradients and introduction of κ_1 and κ_2 yield

$$\frac{i_{ss}}{nFA} = D_1 \frac{c(\ell_1^-) - c(0)}{\ell_1} = D_2 \frac{c(\ell_1 + \ell_2^-) - c(\ell_1^+)}{\ell_2} = D_s \frac{c(\ell_1 + \ell_2 + \delta_0) - c(\ell_1 + \ell_2^+)}{\delta_0} \quad [11]$$

$$= D_2 \frac{c(\ell_1 + \ell_2^-) - c(\ell_1^-)/\kappa_1}{\ell_2} = D_s \frac{c^* - c(\ell_1 + \ell_2^-)/\kappa_2}{\delta_0} \quad [12]$$

For a step to the mass transport limit ($c(0) = 0$), algebra yields $c(\ell_1 + \ell_2^-) = [\frac{D_s}{\delta_0}c^* + \frac{D_2}{\ell_2}\frac{1}{\kappa_1}c(\ell_1^-)]/[\frac{D_2}{\ell_2} + \frac{1}{\kappa_2}\frac{D_s}{\delta_0}]$ and $c(\ell_1^-) = \frac{D_s}{\delta_0}c^*/[\frac{D_1}{\ell_1} + \frac{D_1\ell_2 D_s}{\ell_1 D_2 \kappa_2 \delta_0} + \frac{1}{\kappa_1\kappa_2}\frac{D_s}{\delta_0}]$. On substitution,

$$\frac{i_{ss}}{nFA} = D_1\frac{c(\ell_1^-)}{\ell_1} = \frac{D_1}{\ell_1}\frac{\frac{D_s}{\delta_0}c^*}{\frac{D_1}{\ell_1} + \frac{D_1\ell_2 D_s}{\ell_1 D_2\kappa_2\delta_0} + \frac{1}{\kappa_1\kappa_2}\frac{D_s}{\delta_0}} \quad [13]$$

As for a single film, the Levich plot (i_{ss} versus $\sqrt{\omega}$) is nonlinear. Data analysis is simplified by a double reciprocal (Koutecky Levich) plot. The reciprocal of Equation 13 yields

$$\frac{nFAc^*}{i_{ss}} = \frac{\delta_0}{D_s} + \frac{\ell_1}{\kappa_1\kappa_2 D_1} + \frac{\ell_2}{\kappa_2 D_2} \quad [14]$$

$$\frac{1}{i_{ss}} = \frac{1}{i_{\text{soln}}} + \frac{1}{i_1} + \frac{1}{i_2} \quad [15]$$

The currents i_1 and i_2 represent the currents (proportional to flux) for layers 1 (inner) and 2.

Specification by resistance.—The three layers of solution, outer film, and inner film, each slow probe transport from the solution to the electrode surface. Each layer presents a resistance to mass transport (R_{soln}, R_2, and R_1) and the resistances are in series. By description analogous to a single uniform layer, Equation 15 is found. For series resistance, the measured current can be limited by the highest resistance. For a sufficiently high film resistance, the measured i_{ss} can be ω-independent.

Data analysis.—A plot of i_{ss}^{-1} versus $\omega^{-1/2}$ will yield a linear plot where the slope is characteristic of diffusion in solution and the intercept is $i_1^{-1} + i_2^{-1} = (nFAc^*)^{-1}\left[\frac{\ell_1}{\kappa_1\kappa_2 D_1} + \frac{\ell_2}{\kappa_2 D_2}\right]$. Note κ values also describe probe concentrations prior to electrolysis, $\kappa_2 = c(\ell_1 + \ell_2^-)/c(\ell_1 + \ell^+) = c_2(t = 0)/c^*$ and $\kappa_1\kappa_2 = c(\ell_1^-)/c(\ell_1 + \ell_2^+) = c_1(t = 0)/c^*$. As for the single layer, uniform film, the slopes of the Koutecky Levich plot should be the same for the unmodified and modified electrodes.

The intercept does not allow the permeabilities for the inner ($P_1 = \kappa_1 D_1/\ell_1$) and outer films ($P_2 = \kappa_2 D_2/\ell_2$) to be separated. In principle, coupling the steady state measurement with a transient measurement would allow terms to be separated if thicknesses are known. However, for a bilayer, equations for chronoamperometry and simulations for cyclic voltammetry are not yet reported. Steady state measurements on the bilayer will yield at least a net permeability for the bilayer of $P_1^{-1} + P_2^{-1}$, and variation of ℓ_1 and ℓ_2 may allow separation of some parameter groups. It may be possible to characterize the bilayer by evaluating one layer at a time. In the limit of a very thin ℓ_2 and low κD_2, a bilayer may be characterized as a single layer with measurable $R_{\text{interface}}$.

Example of bilayers.—An excellent paper on multilayers is presented by Rehak and Hall[38] who evaluated bilayers formed of various polymers on a gold electrode and the polymer overlaid with a lipid layer; 1 mM $Fe(CN)_6^{3-}$ was the probe. On initial formation of 3 nm lipid layers over 100 nm sol gel films, Koutecky Levich plots exhibited two different slope domains, where slopes at low ω were the same as the unmodified electrode but as ω increases, slopes increased. After 18 hours, the lipid layer equilibrated to a uniform film and the slopes for all ω were the same as for the unmodified electrode. The permeability of sol gel cured for 10 minute was 4×10^{-10} cm/s, which was twice the value for those cured for 15 minutes. Similar lag times to establish linearity of the Koutecky Levich plots were observed for lipid monolayers over 1-hexadecylamine (HDA) modified 11-mercaptoundecanoic acid (MUA) self assembled monolayers. A smooth surface is needed if the slopes for the unmodified and modified electrodes are to match. The difference in slope at early times and high ω is consistent with surface roughness of the fresh lipid layer before the lipids healed to a lower energy, flat film. For a successful measurement, a film is flat when δ_0 is large compared to any interfacial structural features.

Multilayers, all layers uniform.—Multiple layers built sequentially on an electrode establish different mass transport resistances. At steady state, flux through each layer and the solution must be equal. Algebra can be developed as for the single layer and bilayer, but the same result is found by viewing the system as series mass transport resistances. For n layers on the electrode, allow each j layer to be characterized by ℓ_j, D_j, and κ_j, analogously to above. Series resistances, expressed as currents, i_j, yield

$$\frac{1}{i_{ss}} = \frac{1}{i_{\text{soln}}} + \sum_{j=1}^{n}\frac{1}{i_j} \quad [16]$$

Let the initial concentration in layer j of the film be defined relative to that in the solution as the partition coefficient $\kappa_{j,\text{soln}} = \prod_{k=j}^{n}\kappa_k = \frac{c_j(t=0)}{c^*}$. Then,

$$\frac{nFAc^*}{i_j} = \frac{\ell_j}{\kappa_{j,\text{soln}}D_j} \quad [17]$$

and

$$\frac{nFAc^*}{i_{ss}} = \frac{\delta_0}{D_s} + \sum_{j=1}^{n}\frac{\ell_j}{\kappa_{j,\text{soln}}D_j} = \frac{\delta_0}{D_s} + \sum_{j=1}^{n}\frac{1}{P_j} \quad [18]$$

A Koutecky Levich plot of $nFAc^*i_{ss}^{-1}$ versus $\omega^{-1/2}$ has slope of $[0.62D_s^{2/3}\nu^{-1/6}]^{-1}$ characteristic of solution transport and an intercept proportional to the sum of the mass transport resistance provided by all the layers in the film (Equation 16). The inverse of the last term of Equation 18, $[\sum_{j=1}^{n}P_j^{-1}]^{-1}$ is an effective, net permeability for the multilayer. Absent other information, rotating disk data alone does not allow the parameters for each layer of the film to separated.

Continuously graded layers.—Equation 16 is appropriate for a series of discrete layers. For a continuously graded film, the integral version of Equation 16 is expressed as

$$\frac{nFAc^*}{i_{ss}} = \frac{\delta_0}{D_s} + \int_0^{\ell}\frac{1}{\kappa(\lambda)D(\lambda)}d\lambda \quad [19]$$

ℓ is the total film thickness, λ is the variable of integration, and $\kappa(x)$ and $D(x)$ are the spatially dependent partition and diffusion coefficients that vary normal to the electrode. $\kappa(x)$ parameterizes the initial concentration at point x in the film relative to the bulk solution, c^*. An effective, net permeability for the film is found from the inverse of the intercept. This assumes a mechanically rigid film that does not deform under rotation.

Data analysis.—For any multilayer system, the inverse intercept of the Koutecky Levich plot yields an effective permeability through the multilayer. The plot is indistinguishable from that found by Gough and Leypoldt[12–15] for a uniform single layer. To discriminate multilayers from single layers, additional information such as film formation, imaging studies, and transient voltammetry must be employed to untangle the various system parameters of extraction, diffusion, and thicknesses.

Example of multilayers.—As an example of multilayers, Lu and Hu[39] carefully evaluated permeability of several different multilayers that contain myoglobin (Mb) where the multilayers were assembled electrostatically on pyrolytic graphite electrodes stepwise to set film thickness. All films were established over an initial cationic layer of poly(diallyldimethylammonium), PDDA. The film thickness was parameterized by n, the number of bilayers of Mb + anionic coating layer. Electrodes were modified with either TiO_2 sol gel+Mb [SG-TiO_2/Mb] or TiO_2 nanoparticles +Mb [NP-TiO_2/Mb] or polystyrene +Mb [PSS/Mb]. From quartz crystal microbalance (QCM) studies, the thickness of a single bilayer $\ell_{bilayer}$ ranked as [NP-TiO_2/Mb] (8.4 nm) > [PSS/Mb] (5.0 nm) > [SG-TiO_2/Mb] (3.1 nm). Myoglobin

Table II. Permeability of Fc(COOH) through n Bilayers of Myoglobin (Mb) and TiO_2 Nanoparticles [NP-TiO_2/Mb], Polystyrene, [PSS/Mb] and Sol Gel [SG-TiO_2/Mb].[39]

n	[NP-TiO_2/Mb] $P_{NP-TIO_2/Mb}$ (10^{-3} cm/s)	[PSS/Mb] $P_{PSS/Mb}$ (10^{-3} cm/s)	[SG-TiO_2/Mb] $P_{SG-TIO_2/Mb}$ (10^{-3} cm/s)
1	9.4	6.5	20.3
2	6.3	5.05	14.0
3	5.0	4.2	10.8
4	3.6	3.1	7.2
5	3.1	2.6	5.7
6	3.1	2.3	5.3
7	3.0	2.5	5.0
8			5.1
9			5.0
$\ell_{bilayer}$ (nm)	8.4	5.0	3.1
n_{offset}	0.65	2.2	0.8
P vs $[n - n_{offset}]^{-1}$			
slope (10^{-3} cm/s)	$36._0 \pm 1._8$	$21._5 \pm 1._3$	14.1 ± 0.6
intercept (10^{-3} cm/s)	$0.5_1 \pm 0.4_8$	$-(0.1_6 \pm 0.2_6)$	$0.9_1 \pm 0.2_0$
R^2	0.98_3	0.98_1	0.99_0
$\kappa D_f\|_{eff}$ (10^{-8} cm^2/s)	1.18	1.07	1.12

is electroactive but the reduction potentials for the redox probes ferrocene carboxylic acid is sufficiently positive of myoglobin that the films were electrochemically inert during permeation studies. Values of P for the three types of films captured from Figure 3B in Reference 39 are shown in Table II, where 0.5 mM ferrocene carboxylic acid Fc(COOH) at pH 7 is the probe.

Permeability scales with ℓ^{-1} where ℓ is approximated by n. From the data at the top of Table II for each class of multilayers, P values were linearized to $[n - n_{offset}]^{-1}$ where n_{offset} was optimized to maximize correlation coefficient, R^2. The introduction of n_{offset} improved the regression statistics and included the thickness of the underlying PDDA layer. The value of n_{offset} and slope and intercept of P versus $[n - n_{offset}]^{-1}$ are shown in the Table. In each case, the intercepts approach zero consistent with no significant interfacial resistance. The slopes yield $\kappa D_f n/\ell$, where $\ell/n = \ell_{bilayer}$. An effective $\kappa D_f|_{eff}$ for the multilayers is found as the product of slope and $\ell_{bilayer}$ Listed in Table II, values of $\kappa D_f|_{eff}$, are invariant with types of coating, and average to $(1.12 \pm 0.05) \times 10^{-8}$ cm^2/s. The Mb layers may be the main limitation to flux. Because $\kappa D_f|_{eff}$ is invariant, κ is likely the same in all three films, so that Fc(COOH) has either little electrostatic interaction with NP-TiO_2, PSS, and SG-TiO_2 or interacts only with Mb. If the concentration of Fc(COOH) is the same in the multilayers as it is in solution, then $\kappa \approx 1$ and 1×10^{-8} cm^2/s approximates D_f.

Models for Heterogeneous Films and Composites

For uniform films, the layers are isotropic and only gradients normal to the plane of the electrode affect transport. For heterogeneous films, the layers are not isotropic and the structure varies in the plane of the electrode. Flux of the redox probe is impacted by these structures.

Heterogeneous films and composites are formed of multiple components. Spatially inhomogeneous layers include films with pores and composites of two or more components. Composites include adsorption of one component into a micro- or nano-structured matrix. Heterogeneous films and composites are differentiated from uniform films by a microstructural characteristic dimension parallel to the plane of the electrode, where the characteristic dimension is either comparable to or smaller than either ℓ or δ_0. As the characteristic dimension approaches molecular to nanoscale and is substantially smaller than ℓ and δ_0, films will be characterized as uniform by rotating disk voltammetry. To model steady state voltammetry for heterogeneous films and composites, mass transport resistance applies.

Specification by resistance.—In sections Specification by resistance in single layer, uniform films, Specification by resistance in bilayers, two uniform layers, and Multilayers, all layers uniform, steady state current measured through uniform films is modeled as mass transport resistance. Probe motion through the homogeneous solution is resisted by probe interactions with the electrolyte. Addition of a film leads to additional resistances For uniform, incompressible films, mass transport is captured as serial resistances because net transport is only normal to the electrode. Equation 16 for multilayer films also captures single and bilayer films, $i_{ss}^{-1} = i_{\text{soln}}^{-1} + \sum_{j=1}^{n} i_j^{-1}$. Current is related to flux, J as $i/nF = -AJ$, where any current, i_k, is proportional to the flux J_k across the cross sectional area A_k where J_k is established. For unmodified electrodes and uniform films, the cross sectional area is the electrode area, A. Thus, for the series mass transport resistances for uniform films, substitution into Equation 16 yields

$$(J_{total}A)^{-1} = (J_{soln}A)^{-1} + \sum_{j=1}^{n}(J_jA)^{-1} \quad [20]$$

$$J_{total}{}^{-1} = J_{soln}{}^{-1} + \sum_{j=1}^{n} J_j{}^{-1} \quad [21]$$

Consider a nonuniform, heterogenous film composed of two materials a and b where each has a cross section, A_a and A_b, in the plane of the electrode. Components a and b can each be distributed in numerous small domains across total area A but the sum of the total cross section of each is such that $A = A_a + A_b$. An example is an array of colinear, cylindrical pores that traverse a support. A probe moves through the material where components a and b provide two parallel paths through the layer. Each component provides resistance to mass transport R_a and R_b. Because the resistances are in parallel, mass transport resistance through the film is $R_{film,total}^{-1} = R_a^{-1} + R_b^{-1}$. For parallel currents in the film, $i_{film,total} = i_a + i_b$. On substitution of $i_j = -nFA_jJ_j$,

$$AJ_{film,total} = A_aJ_a + A_bJ_b \quad [22]$$

$$J_{film,total} = \frac{A_a}{A}J_a + \frac{A_b}{A}J_b \quad [23]$$

$$= f_aJ_a + f_bJ_b \quad [24]$$

f_a and f_b are the fractional cross sectional areas of each component, $f_k = A_k/A$. For multiple components, total flux in the film is set by the flux of each component J_k and the fractional cross sectional area f_k through which J_k is established, where $\sum_k f_k = 1$.

$$J_{film,total} = \sum_k f_kJ_k \quad [25]$$

If there is a non-permeable component on the electrode, its fractional area is included but its flux is zero. For a multicomponent, heterogeneous film on an electrode, mass transport resistance for the solution and entire film remains serial, $R_{total} = R_{soln} + R_{film,total}$. The corresponding currents are $i_{total}^{-1} = i_{soln}^{-1} + i_{film,total}^{-1}$. For each i_{total}, i_{soln}, and $i_{film,total}$, the total cross section is the geometric area of the electrode, A.

$$J_{total}{}^{-1} = J_{soln}{}^{-1} + J_{film,total}{}^{-1} \quad [26]$$

On substitution of $J_{film,total} = \sum_k f_kJ_k$ for a heterogeneous film, Equation 26 yields

$$J_{total}{}^{-1} = J_{soln}{}^{-1} + \frac{1}{\sum_k f_kJ_k} \quad [27]$$

Because transport in solution is not perturbed by the modifying layer and there are no reaction kinetics, the slope of the Koutecky Levich plot remains the same as for the unmodified electrode. The intercept characterizes $[\sum_k f_kJ_k]^{-1}$. If data are collected where f_k is varied in a known manner, J_k through each component can be

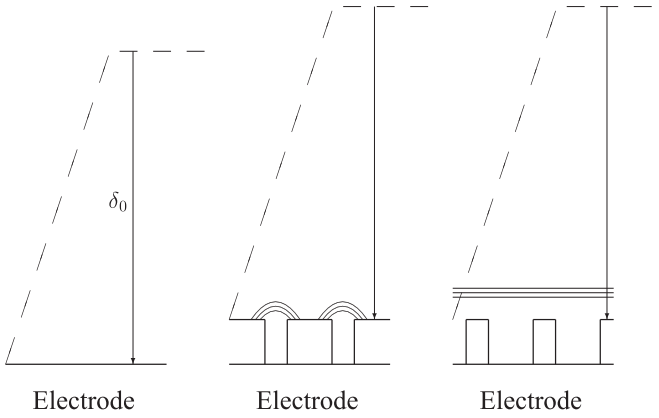

Figure 2. The boundary layer of thickness δ_0 is shown as dash at an unmodified electrode and at electrodes modified with layers containing pinholes. Measurements by rotating disk voltammetry map the transit of a probe from the outer edge of the boundary layer to the electrode surface. For the unmodified electrode, the path is normal to the electrode, as shown by the vector. When the electrode is modified with a layer containing pinholes, the probe moves from outside the boundary layer to the electrode surface but the path of the probe may be blocked by material on the electrode. If δ_0 is large compared to the features in the film, then the deviation in the path of the probe to the electrode is negligible. For the case of small pinholes well separated (middle panel), the radial diffusion layer is small compared to δ_0 and rotating disk data yield an effective permeability. In the case of large pinholes, the radial diffusion profiles merge to a linear profile a short distance from the layer as shown in the right panel. Where the merged diffusion layer is thin compared to δ_0, the path of the probe is lengthened neglibly as the probe reaches the electrode and effective permeability is again measured.

determined by evaluating total flux as a function of the characteristic dimensions that set f_k.

Pores and microstructured composites.—Rotating disk voltammetry measures effective permeability through layers that contain pores and other regular micro- and nano-structural components. Effective permeability is measured once the boundary layer, δ_0, is approximately five times the largest characteristic dimension of the structures in the plane of the electrode. Like concentration profiles at microelectrodes, steady state, boundary layers that perturb concentration from bulk drop across a distance less than five electrode radii.

For straight, colinear pores of radius r at a density of N pores per cm^2 and pores separated center to center by $2R$ at steady state, a radial diffusion profile of length $\sim 5r$ is established about each pore at the film solution interface, if the pores are well separated. See the middle panel of Figure 2. If pores are not well separated, the radial diffusion profiles merge into a linear diffusion profile, as shown in the right panel of Figure 2. As long as either $5r$ or the linear diffusion profile formed as the radial profiles merge have characteristic lengths well less than δ_0, rotating disk will yield an effective permeability P. The diffusion path for probes diffusing across δ_0 will be negligibly lengthened compared to the normal by the film structures on the electrode. A rough estimate of a sufficiently thick boundary layer is that δ_0 exceeds five times the dimension of the largest structural feature, so that the probe diffusion path differs negligibly from the normal and the effective permeability is measured. For colinear, cylindrical pores, $2R > r$, so $2R$ sets one diffusion length. As long as $\delta_0 \gtrsim 10R$, probes diffusing from $\delta_0 + \ell$ to ℓ will establish diffusion paths near normal to the electrode, so effective permeability is measured. For cases where $2R$ and r are comparable to δ_0, Landsberg and coworkers[35,40,41] derived the equations for pinholes.

For straight pores through an inert substrate, the porosity ε is the open cross section of the pores normalized by A, $\varepsilon = \pi N r^2/A$; ε is the same as f_{open}. Expressed in terms of surface coverage, θ, $\varepsilon = 1-\theta$. If the pores are solution filled, a linear concentration gradient within the pores yields $-J_{film} = \varepsilon D_s/\ell$. For pores filled with material other than solution,[42,43]

$$-J_{film} = \frac{i_{film}}{nFA} = \frac{\kappa D_f}{\ell}\varepsilon = P\varepsilon \qquad [28]$$

If a film contains pores of uniform radius r separated by $2R$ center to center, but the pores are not straight, the above equations apply when modified for the tortuosity, $\tau = pore\ length/\ell$ as

$$\frac{i_{film}}{nFA} = \frac{\kappa D_f}{\ell}\frac{\varepsilon}{\tau} = P\frac{\varepsilon}{\tau} \qquad [29]$$

where $\tau\ell$ is the path length for diffusion through the film.

If permeabilities are determined as a function of the composition and dimensions of the microstructural components, additional information about mass transport associated with the microstructures can be extracted.[43,44]

When δ_0 is comparable to the scale of the microstructural characteristic lengths, these analyses will likely fail. Under these conditions, scanning electrochemical microscopy (SECM), first introduced by Bard and coworkers,[45] may be appropriate as SECM exploits interrogation of the boundary layers established about micro- to nanostructures. Quantitative aspects of SECM measurements have been described by Cornut and Lefrou.[46] For rotating disk measurement, if δ_0 can be increased to several fold the microstructural characteristic lengths, then effective porosity of the layer can be measured. These methods may be useful in characterizing films with characteristic dimensions that approach molecular such as well formed films of zeolites and covalent (COF) and metal organic (MOF) frameworks. Transport around and through the structures must be differentiated as has been undertaken for clay films on electrodes.[6] At the other extreme, δ_0 may not be large compared to structural features and measurement constraints are not satisfied; for example, non-linear Koutecky Levich plots are sometimes observed for large pinholes and rough surfaces.

Limitations of the Measurements

When compared to an unmodified electrode, the presence of a film or membrane on the electrode surface alters the time to achieve steady state and the allowed rotation rates. It also introduces some statistical limitations on the data analysis.

Time to steady state.—The presence of a film on the electrode introduces a lag time to establish steady state because physical diffusion coefficients within films are often many orders of magnitude lower than diffusion coefficients in solution. The time needed to achieve steady state is again set by approximately five times the diffusion length, $t_{ss} \gtrsim 5\ell^2/D_f$. As ℓ increases, the time to steady state increases dramatically. For example, in Nafion films of a micrometer thickness, the time to achieve steady state is on the order of a few hours.[47] Experimentally, the time to achieve steady state is found by applying a fixed potential and monitoring the current until it is invariant. Measurements are most efficiently made by maintaining the electrode at this potential when changing ω. Scanning the potential for each ω complicates determining whether the system is at steady state. Once films are characterized, comparison of the values ℓ and D_f to the time to steady state serves as a crude check of measurement quality.

Rotation rates.—At unmodified electrodes, the upper limit on ω is set by the onset of turbulence. The lower limit is set when the hydrodynamic boundary layer thickness exceeds the radius of the disk electrode[20] as $\omega > 10\nu/r_{disk}^2$. For modified electrodes, the upper limit on ω is similarly set. Practical experience has shown that the lower limit of ω is lower than for an unmodified electrode. For example, Nafion modified electrodes can be studied at a few rotations per minute. Slower rotation rates may be achieved when the mass transport resistance in the film is high compared to that in the solution.

Surface roughness.—In vetting measurements on modified electrodes, good measurements require δ_0 large compared to characteristic lengths for structures in the layer, as in Figure 2. When the coating on the electrode is not flat and has features of lengths comparable to δ_0, then the rotating disk measurement may not be useful. The boundary layer is established as solvent molecules are carried by the flat rotating surface. If the layer is not flat, then solvent will be trapped in the valleys at the film solvent interface and the boundary layer will be superimposed above the entrapped solvent. Because the zone of entrapped solvent is poorly defined, the Koutecky Levich analysis does not serve to characterize the film. If linear, the slopes may deviate from those in solution. Large pinholes where δ_0 is not sufficiently large cause non-linear Koutecky Levich plots especially at higher ω. Examples are noted in References 34, 38.

Statistical limitations.—Where the Koutecky Levich equation characterizes current, $i_{ss}^{-1} = i_{\text{soln}}^{-1} + i_{film}^{-1}$, i_{film} embeds the permeability, whether that is the permeability or the effective net permeability for the layer. When mass transport resistances for the film and solution are comparable, such that both i_{soln}^{-1} and i_{film}^{-1} are significant, the Koutecky Levich plot yields an ω-dependent slope that is the same as that for the unmodified electrode and an ω-independent intercept characteristic of film flux. In some cases, flux in the film is so low that $i_{film}^{-1} \gg i_{\text{soln}}^{-1}$ and within the experimental uncertainties, i_{ss} is limited solely by film flux. The Koutecky Levich plot will be ω-independent and $i_{ss} = i_{film}$. It is sometimes observed that the Koutecky Levich plot is linear, but the slope falls between that for the unmodified electrode and zero. This may occur where film flux is substantially less than solution flux but not yet small enough that the measured current is ω-independent. For small currents, measurement precision can obscure the ω dependence. When $i_{film} \ll i_{\text{soln}}$ but i_{ss} is not yet ω-independent, several factors can adversely impact measurement quality. When i_{film} is low, long t_{ss} is common; if insufficient time is allowed to achieve steady state, then the steady state model is not applicable because $J_{film} \neq J_{\text{soln}}$ and i_{ss} will be overestimate at given ω. If steady state is achieved, the model constrains $J_{film} = J_{\text{soln}}$, where small J_{film} requires extremely long δ_0 be established at very low ω. If for example, density gradients and thermal motion disrupt the boundary layer, the measurement boundary layer δ_0' is thinner than the intended δ_0 based on applied ω and the measured i_{ss}' will be higher than the i_{ss} that correlates with δ_0. When i_{ss}' is analyzed with δ_0, both the Levich and Koutecky Levich plots can be misinterpreted.

A simplistic representation of boundary layer disruption on Koutecky Levich plots is shown in Figure 3, where data are calculated for common experimental conditions in water. The plot of $nFAc^*D_s/i_{ss}$ versus δ_0 for the unmodified electrode is shown by the open gray circles and the solid gray regression line, with slope $m_{KL,un\,\text{mod}}$ and intercept zero. When a uniform film with $P = 3.2 \times 10^{-3}$ cm²/s is added, the plot shown with solid gray circles and a thin solid line results with slope $m_{KL,un\,\text{mod}}$ and intercept P^{-1}, as anticipated for films evaluated well within model constraints. Koutecky Levich plots are shown for a simple model where the boundary layers at all ω are decreased with fixed δ_0'/δ_0. For $\delta_0'/\delta_0 = 0.99$, the long dashed line (slope $0.99m_{KL,un\,\text{mod}}$) is nearly coincident with the film with slope $m_{KL,un\,\text{mod}}$. As δ_0'/δ_0 decreases, plots are linear of slope $(\delta_0'/\delta_0)m_{KL,un\,\text{mod}}$. For the smallest δ_0'/δ_0, the slope approaches zero. Here, all lines converge to intercept P^{-1}, but this is an artifact of the simple model as posed. In experiments, the extent of boundary layer disruption will likely increase with thickness ($\omega^{-1/2}$). A range of slopes between $m_{KL,un\,\text{mod}}$ and zero maps behavior between those anticipated based on the model and a film flux so low that the ω dependence is lost to the precision of the measurements.

Koutecky Levich plots that have slopes less than the solution slope but greater than zero do not allow ready measurement of film permeability. Experimentally, changing the range of ω or ℓ by an order of magnitude may shift the behavior into either ω independence or ω dependence of the unmodified electrode. When lower ω values experimentally accessible for modified electrodes are used, verify the Koutecky Levich slope is the same as $m_{KL,un\,\text{mod}}$. For poorly resolved Koutecky Levich plots, a Levich plot of i_{ss} versus $\omega^{1/2}$ may be more appropriate, where i_{film} is extrapolated to the limiting i_{ss} at infinite ω.

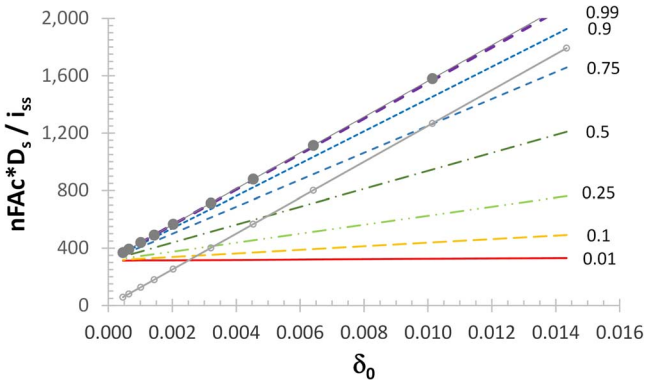

Figure 3. Koutecky Levich plots are represented for the unmodified electrode of slope $m_{KL,un\,\text{mod}}$ and intercept zero (gray open circles, solid gray regression line); a film of $P = 3.2 \times 10^{-3}$ cm/s with slope $m_{KL,un\,\text{mod}}$ and intercept P^{-1}; and a series of examples where disruption of the boundary layer by thermal motion and density gradients leads to a decrease in the experimental boundary layer thickness δ_0' as compared to the intended δ_0 associated with the experimental ω. As δ_0'/δ_0 (the labels for the lines) decreases, slope decreases as $(\delta_0'/\delta_0)m_{KL,un\,\text{mod}}$. (For illustration, the simplistic model is that δ_0'/δ_0 is the same for all ω.) The disruption in the boundary decreases the slope. The common intercept P^{-1} is an artifact of the simple model; P^{-1} is not anticipated well measured from experimental data. The plot is based on water at room temperature, a common P, and D_s of 8×10^{-6} cm²/s.

In cases where the Koutecky Levich plot is ω-independent and slope zero, $J_{film} \ll J_{\text{soln}}$ and the measured $i_{ss} = i_{film}$. Thus, if data are ω-independent, then the film is still parameterized by rotating disk. Time to steady state may be long.

Non-linear Koutecky Levich plots.—Koutecky Levich plots may be nonlinear, even when rotation rates are appropriate. Non-linear plots arise when the model for series mass transport resistances fails. Non-linear effects include kinetic effects for reactions within the films, such as those described by Albery[48] and Savéant and coworkers.[24,49–54] Effects other than transport in the solution that are rotation rate dependent can yield plots that are either non-linear or have a Koutecky Levich slope other than that observed for the unmodified electrode. A film that is fluid and distorts on rotation because of shear would not be well described by the Koutecky Levich analyses.[55] Pinholes and surface roughness can yield non-linear Koutecky Levich plots.

Conclusions

The well-controlled mass transport established at steady state rotating disk electrodes yields excellent conditions for determination of flux through films and membranes. Because of the highly effective stirring, measurements are more reliable and less hazardous than radiotracer methods. Gough and Leypoldt[12–15] first presented the equation characteristic of steady state transport of a redox probe from solution through a homogeneous film to the electrode where the probe undergoes diffusion limited electrolysis. Measurements are made on electrochemically inert films that are either not electroactive or evaluated in a voltage range where the film is not electrolyzed. Here, equations are presented to characterize flux through bi- and multilayers that include discretely and continuously graded films. When only rotating disk voltammetric data are used and other information about the layers is absent (e.g., thicknesses), only an effective permeability through the film is found. Discussion of the conditions where rotating disk voltammetry can be used to characterize microstructured films and films with pores is presented.

Electrodes modified with multilayers can be characterized by rotating disk voltammetry and Koutecky Levich (i_{ss} (ω)$^{-1}$ versus $\omega^{-1/2}$)

plots. Intercept of linear plots yields an effective permeability through the layers but, in the absence of other information or transient voltammetric results, neither the permeabilities that characterize the individual layers nor the three characteristics of partition parameter, diffusion coefficient, and film thickness can be determined separately. Heterogeneous films can also be characterized by Koutecky Levich analyses provided the characteristic dimensions of the film structures are well below the thickness of the boundary layer, δ_0. Modified electrodes require longer times to establish steady state but measurements can be made at lower rotation rates. Two conditions allow ready determination of permeability, where either the mass transport resistance in the film and solution are comparable or where the mass transport resistance in the film is dominant and the steady state current is ω-independent. Intermediate cases are not well interpreted. Change of ℓ or ω may shift results into either i_{film} comparable to i_{soln} or $i_{film} \ll i_{soln}$. Limitations to the method include nonlinear Koutecky Levich plots that can arise from several factors that include reactions within the films, films sufficiently fluid that the film distorts on rotation, and large pinholes. Consideration of serial and parallel mass transport resistances in the layer generates diagnostics appropriate to the film microstructure.

Acknowledgments

The financial assistance of the Army Research Office (ARO 43808-CH / DAAD19-02-1-0443) and the National Science Foundation (NSF 1309366) are most gratefully acknowledged. A Fellowship in Residence at the Obermann Center for Advanced Studies facilitated completion of this paper. Dedicated to Allen J. Bard on the occassion of awarding the first Allen J. Bard Award of the Electrochemical Society, 2015.

References

1. R. Murray, *Acc. Chem. Res*, **13**, 135 (1980).
2. R. Murray, *Molecular Design of Electrode Surfaces* Vol. 22 of *Techniques of Chemistry*, Interscience, New York, (1992).
3. M. Kaneko and D. Worhle, *Adv. Polym. Sci*, **84**, 141 (1988).
4. H. Abruna, *Coord. Chem. Rev.*, **86**, 135 (1986).
5. K. Snell and A. Keenan, *Chem. Soc. Rev.*, **8**, 259 (1979).
6. A. Fitch, *Clays and Clay Minerals*, **38**, 391 (1990).
7. R. Durst, A. Baumner, R. Murray, R. Buck, and C. Andrieux, *Pure and Appl. Chem*, **69**, 1317 (1997).
8. M. Opallo and A. A. Lesniewski, *J. Electroanal. Chem.*, **656**, 2 (2011).
9. P. Cervini and E. Cavalheiro, *Analytical Letters*, **45**, 297 (2012).
10. A. Walcarius, *Analytica Chimica Acta*, **384**, 1 (1999).
11. S. Bruckenstein and B. Miller, *Acc. Chem. Res*, **10**, 54 (1977).
12. D. Gough and J. Leypoldt, *Anal. Chem.*, **51**, 439 (1979).
13. D. Gough and J. Leypoldt, *A.I. Ch. E. J.*, **26**, 1013 (1980).
14. D. Gough and J. Leypoldt, *Anal. Chem.*, **52**, 1126 (1980).
15. D. A. Gough and J. K. Leypoldt, *J. Electrochem. Soc.*, **127**, 1278 (1980).
16. C. M. Carlin, L. J. Kepley, and A. J. Bard, *J. Electrochem. Soc.*, **132**, 353 (1985).
17. S. Bruckenstein and A. R. Hillman, Electrochemical quartz crystal microbalance studies of electroactive surface films, in *Handbook of Surface Imaging and Visualization*, A. T. Hubbard, Editor, CRC Press, Boca Raton, FL, 101–13 (1995).
18. D. A. Buttry and M. D. Ward, *Chem. Rev.*, **92**, 1355 (1992).
19. J. Leddy and A. J. Bard, *J. Electroanal. Chem.*, **153**, 223 (1983).
20. A. Bard and L. Faulkner, *Electrochemical Methods*, John Wiley & Sons, Inc., New York, (2001) Second ed.
21. A. Amarasinghe, T. Chen, H. Paul, P. Moberg, F. Tinoco, L. Zook, and J. Leddy, *Anal. Chim. ACTA*, **307**, 227 (1995).
22. P. Peerce and A. Bard, *J. Electroanal. Chem.*, **112**, 97 (1980).
23. K. L. Knoche, C. Hettige, P. D. Moberg, S. Amarasinghe, and J. Leddy, *J. Electrochem. Soc.*, **16** H285 (2013).
24. J. Leddy, A. Bard, J. Maloy, and J. Saveant, *J. Electroanal. Chem.*, **187**, 205 (1985).
25. M. Krishnan, X. Zhang, and A. J. Bard, *J. Am. Chem. Soc*, **106**, 7371 (1984).
26. D. Ege, P. K. Ghosh, J. R. White, J.-F. Equey, and A. J. Bard, *J. Am. Chem. Soc*, **107**, 5644 (1985).
27. P. Henning, H. S. White, and A. J. Bard, *J. Am. Chem. Soc*, **104**, 5862 (1982).
28. R. A. Bull, F.-R. Fan, and A. J. Bard, *J. Electrochem. Soc.*, **131**, 687 (1984).
29. R. Bull, F.-R. Fan, and A. Bard, *J. Electrochem. Soc.*, **130**, 1636 (1983).
30. J. Leddy and A. Bard, *J. Electroanal. Chem.*, **153**, 223 (1983).
31. J. Leddy and A. Bard, *J. Electroanal. Chem.*, **189**, 203 (1985).
32. X. Zhang, J. Leddy, and A. Bard, *J. Am. Chem. Soc*, **107**, 3719 (1985).
33. T. Okajima, T. Ohsaka, O. Hatozaki, and N. Oyama, *Electrochimica Acta*, **37**, 1865 (1992).
34. J. J. Gooding, C. E. Hall, and E. A. H. Hall, *Analytica Chimica Acta*, **349**, 131 (1997).
35. R. Landsberg and R. Thiele, *Electrochimica Acta*, **11**, 1243 (1966).
36. S. Cosnier, S. Szuneritus, R. S. Marks, A. Novoa, L. Pueh, E. Peres, and I. Rico-Lattes, *Talanta*, **55**, 889 (2001).
37. T. Ikeda, R. Schmehl, P. Denisevich, K. Willman, and R. W. Murray, *J. Am. Chem. Soc*, **104**, 2683 (1982).
38. M. Rehak and E. A. H. Hall, *Analyst*, **129**, 1014 (2004).
39. H. Lu and H. Naifei, *Electroanalysis*, **15**, 1511 (2006).
40. F. Scheller, S. Muller, R. Landsberg, and H.-J. Spitzer, *J. Electroanal. Chem.*, **19**, 187 (1968).
41. F. Scheller, R. Landsberg, and S. Muller, *J. Electroanal. Chem.*, **20**, 375 (1969).
42. J. Leddy and N. E. Vanderborgh, *J. Electroanal. Chem.*, **235**, 299 (1987).
43. Y. Fang and J. Leddy, *J. Phys. Chem.*, **99**, 6064 (1995).
44. L. A. Zook and J. Leddy, *J. Phys. Chem. B*, **102**, 10013 (1998).
45. A. J. Bard, F. R. F. Fan, J. Kwak, and O. Lev, *Anal. Chem.*, **61**, 132 (1989).
46. C. Lefrou and R. Cornut, *ChemPhysChem*, **11**, 547 (2010).
47. L. A. Zook, *Morphological Modification of Nafion For Improved Electrochemical Flux*, Ph.D. thesis, University of Iowa, 1996 (1996).
48. W. Albery and A. Hillman, *Annu. Rep. Prog. Chem., Sect. C*, **78**, 377 (1981).
49. C. P. Andrieux and J. M. Saveant, Catalysis at Redox Polymer Coated Electrodes, in *Molecular Design of Electrode Surfaces*, R. W. Murray, Editor, Vol. XXII John Wiley & Sons, Inc., New York, 207–270 (1992).
50. C. Andrieux, J. Dumas-Bouchiat, and J. M. Saveant, *J. Electroanal. Chem.*, **131**, 1 (1982).
51. C. Andrieux and J. Saveant, *J. Electroanal. Chem.*, **142**, 1 (1982).
52. C. Andrieux, J. Dumas-Bouchiat, and J. Saveant, *J. Electroanal. Chem.*, **169**, 9 (1984).
53. C. Andrieux and J. Saveant, *J. Electroanal. Chem.*, **171**65 (1984).
54. C. P. Andrieux and J. M. Saveant, *J. Electroanal. Chem.*, **134**, 163 (1982).
55. A. Oron, S. H. Davis, and S. G. Bankoff, *Reviews of Modern Physics*, **69**, 931 (1997).